PERGAMON

International Journal of Solids and Structures 36 (1999) 5357–5385

INTERNATIONAL JOURNAL OF SOLIDS and STRUCTURES

www.elsevier.com/locate/ijsolstr

Point attractors and dynamic buckling of autonomous systems under step loading

D.S. Sophianopoulos

Metal Structures Laboratory, Department of Civil Engineering, National Technical University of Athens, 42 Patision St., 106 82 Athens, Greece

Received 7 October 1997; in revised form 24 July 1998; accepted 10 August 1998

Abstract

In this study the dynamic response of autonomous mainly dissipative multi D.O.F. systems under step loading is re-examined. Based on the geometrical point of view of the theory of non-linear dynamical systems and the rapidly developing theory of attractors, the investigation focuses on limit point like systems, with snapping as their salient feature. It is found that dynamic buckling (through a saddle or its neighborhood), although leading to a large amplitude motion, may be associated with a point attractor response on the pre-buckling fixed point, depending on the amount of damping considered in close conjunction with the motion channel geometry and the total potential characteristics of all (stable and complementary) equilibria. For such systems, only a straightforward fully non-linear dynamic analysis can provide valid information on the global dynamic stability, since the shape of the total potential hypersurface may become very complicated, rendering energy aspects practically not applicable. A 2-D.O.F. model, simulating an asymmetric suspended roof is comprehensively analyzed to capture the above findings, and a parametric investigation is carried out, revealing a variety of new dynamic response types and leading to a more accurate insight of the stability of motion in the large.

1. Introduction

According to recent studies on the nonlinear dynamic stability of autonomous dissipative/nondissipative potential structural systems (Gantes and Kounadis, 1995; Kounadis, 1993a; 1996), on the basis of topological, geometrical as well as energy aspects, dynamic buckling (under step, impulsive or impact loading) is defined as that state, for which an escaped motion occurs, due to an infinitesimal increase of the loading; this takes place through a particular fixed point (or its vicinity), being simultaneously a saddle of both the total potential energy surface (in the V-displacement space) and of the loading surface (in the load-displacement space). The aforementioned studies have also shown that this saddle (with negative total potential energy) may belong either to an unstable branch of the natural post-buckling equilibrium path (for limit point systems) or to unstable complementary paths (for statically stable or imperfection-sensitive

0020-7683/98/$ - see front matter
PII: S0020-7683(98)00249-2

systems); moreover, when the amplitude of motion or the boundary of the basin of attraction of a stable prebuckling equilibrium point touches one of these unstable paths (with $V < 0$), all the conditions for the initiation of the dynamic buckling mechanism are fulfilled and consequently the system's motion escapes through the saddle (or its neighborhood).

In the existing relevant literature, after the instant of dynamic buckling there are two types of possible dynamic response that are reported. One is associated with a point attractor response on a remote postbuckling natural (or sometimes complementary) stable equilibrium, while the motion is unable to return backwards through the saddle (following an opposite direction), and the other with an unbounded motion (when no postbuckling stable equilibrium configurations exist or the ones existing are not 'strong' enough to eventually trap and capture the motion).

The present investigation, extending the previous significant findings, reveals a third possibility of dynamic postbuckling response, associated with a point attractor on the pre-buckling natural fixed point; based on the geometrical point of view and basic definitions of the theory of nonlinear dynamical systems, the whole analysis focuses on the overall geometrical and energy properties of all stable (natural as well as complementary) equilibria, corresponding to loads equal or higher than the dynamic buckling one, and to special cases of limit point systems with always negative total potential (along the physical equilibrium path). The new findings are verified through a straightforward nonlinear dynamic analysis of a 2-D.O.F. autonomous system under step conservative loading of infinite duration, simulating an asymmetrical suspended roof. A variety of numerical results in graphical form validate the theoretical predictions, while qualitative considerations accompanying the whole study bring a more comprehensive conception of stability of motion in the large.

2. Theoretical aspects

Let us consider a general n-degree of freedom autonomous dissipative structural system, subjected to a step constant directional (conservative) loading λ of infinite duration. The Lagrange equations governing the system's motion, in terms of its generalized coordinates $q_i(t)$ and velocities $\dot{q}_i(t)$ are given by the well known relation:

$$\frac{d}{dt}\left[\frac{\partial K}{\partial \dot{q}_i}\right] - \frac{\partial K}{\partial q_i} + \frac{\partial V}{\partial q_i} + \frac{\partial F}{\partial \dot{q}_i} = 0 \quad (i = 1, 2, \ldots, n) \tag{1}$$

where K is the positive definite function of the total kinetic energy, V the total potential and F is Rayleigh's dissipation function. For an imperfect system initially at rest, i.e. satisfying the following initial conditions

$$q_i(0) = q_i^0, \quad \dot{q}_i(0) = 0, \quad (i = 1, 2, \ldots, n) \tag{2}$$

it can be readily proven that function $E = K + V + 2\int_0^t F\,\mathrm{d}t'$ is constant throughout the motion (Huseyin, 1981; Kounadis, 1993a), but rarely analytic.

Setting $x_1 = q_1, x_2 = q_2, \ldots, x_n = q_n, x_{n+1} = \dot{q}_1, \ldots, x_{2n} = \dot{q}_n$ the system of eqns (1) can be written in a matrix-vector form as follows:

$$\dot{\mathbf{x}} = f(\mathbf{x},\lambda), \quad \mathbf{x}(x=0) = \mathbf{x}_0 \tag{3}$$

with λ being the main control parameter.

This can be treated as the state eqn of a $2n$-th order autonomous nonlinear dynamical system, with vector field $\mathbf{x}: R^{2n} \rightarrow R^{2n}$. Such a system can be comprehensively classified in terms of its steady-state solutions and limit sets. Adopting some basic definitions of the theory of nonlinear dynamical systems, such as the ones of limit point $\mathbf{y}$ and attracting limit set L (Guckenheimer and Holmes, 1983; Parker and Chua, 1987; Wiggins, 1980), the domain (basin of attraction) $B(L)$ of L is the union of all open neighborhoods U of L, for which $L(x) = L, \forall x \in U$. Thus, every trajectory starting in $B(L)$ tends towards L as $t \rightarrow \infty$. The latter gives a first approach to the concept of attractors (Rouelle, 1981), which are precisely defined as topologically transitive attracting sets (Milnor, 1985; Wiggins, 1980). For autonomous Hamiltonian systems, as the one dealt with, the only type of steady-state behavior—and the simplest limit set case—is the equilibrium (fixed) point $\mathbf{x}_E$, given by:

$$f(\mathbf{x}_E) = 0. \tag{4}$$

Equation (3) then yields

$$\frac{\partial V}{\partial x_i}(x_i;\lambda) = 0 \quad (i = 1,2,\ldots,n) \tag{5}$$

constituting a necessary and sufficient criterion for static equilibrium.

Furthermore, since for Hamiltonian systems (Moser, 1968) equilibria are not affected by damping, all orbits (i.e. the system's motion itself) (Wiggins, 1980) are restricted to lie in $(2n-1)$ dimensional 'energy' (hyper)surfaces given by the level sets of the Hamiltonian, being in fact the sum of V and K. These surfaces are the union of the domains of all attracting limit sets (in this case equilibria), corresponding to all acceptable levels of $V(\leqslant 0)$, and inside these lie all the fixed points resulting from the solution of eqn (5) for the chosen value of λ. Stable equilibria are relative minima of the aforementioned surfaces (wells), while saddles (if existing) are relative maxima (hilltops) (Dubrovin et al., 1984a; 1984b). These saddles are non-stable, remaining that way even if the flow is reversed, contrary to unstable points, which become stable in reverse time (sources $\leftrightarrow$ sinks).

For the simple case of a limit point system, with snapping as its main feature, at the instant and after dynamic buckling, i.e. for values of the loading λ: $\lambda_{DD} \leqslant \lambda < \lambda_S$ (where λ_{DD} is the exact dynamic buckling load of the damped system and λ_s the corresponding limit point load) the energy surface is in most relevant systems associated with two domains interconnected in the neighborhood of a saddle. One domain belongs to the natural stable prebuckling equilibrium and the other to a remote stable postbuckling equilibrium configuration. From a purely qualitative point of view, and based on the characteristics of saddles, as defined previously, the motion may as well find its way through the vicinity of the saddle from one basin of attraction to the other from both available directions. Consequently, which stable fixed point will eventually act as an attractor depends not only on the geometry of the first (prebuckling) domain, where the motion starts, but also on the overall surface structure of the second (postbuckling) domain, and of course on the number of degrees of freedom (restricting the motion when increased) and the amount of damping considered.

On the other hand, if one considers a far more complicated case, associated with multiple

domains (i.e. stable fixed points for the same loading, physical and complementary) and saddles, then the motion has many choices and the dimensions and surface structure of all basins of attraction must be accounted for, in order to finally determine where (in the presence of damping) the system will rest as $t\to\infty$, a fact guaranteed from the theory of attractors (Milnor, 1985). Additionally, if all the above are combined with always negative total potential, implying motion, the well known zero V_T criterion (Kounadis, 1993b) can not be readily applied; thus neither lower bound dynamic buckling estimates nor the direction of motion and its global response can be established on the basis of energy approach. Apparently, only a straightforward nonlinear dynamic analysis can provide accurate information about global dynamic stability; this is so especially because the most governing nonlinear terms are not a priori known and seeking a normal form (Guckenheimer and Holmes, 1983; Ruelle, 1981; Wiggins, 1980) will rather complicate than simplify the whole investigation.

All the above theoretical qualitative findings will be verified below, through the comprehensive fully nonlinear (static as well as) dynamic stability analysis of a 2-D.O.F autonomous potential system, simulating an asymmetrical suspended roof under step loading (Michaltsos and Sophianopoulos, 1998).

3. Illustrative example

Let us consider the imperfect 2-D.O.F. dissipative system depicted in Fig. 1., used in the recent literature (Michaltsos and Sophianopoulos, 1998) for the simulation of an asymmetrical suspended roof ($\alpha_1\neq\alpha_2$ in general). This particular model consists of three springs K_i with corresponding dashpots C_i and a concentrated mass m, being initially at rest at the deformed configuration $AB\Gamma'$

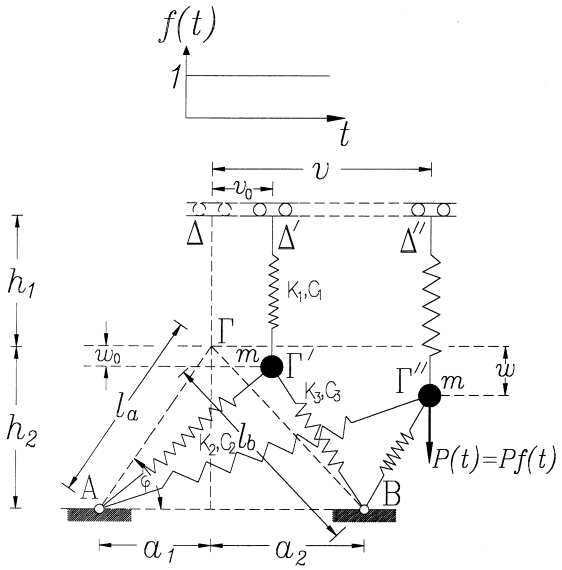

Fig. 1. Two degrees of freedom model simulating an asymmetrical suspended roof.

Δ', where all springs are considered unstressed. Note that A, B are immovable hinges, while support Δ can freely slide along horizontal tracks, and thus spring 1 remains always vertical. At this state, if w_0 and υ_0 are the initial vertical and horizontal displacement components respectively, the lengths of the model's springs are equal to:

$$l_1 = h_1 + w_0$$

$$l_2 = [(a_1 + \upsilon_0)^2 + (h_2 - w_0)^2]^{1/2} = \beta_2 l_a, l_3 = [(a_2 - \upsilon_0)^2 + (h_2 - w_0)^2]^{1/2} = \beta_3 l_a \tag{6}$$

If the system is acted upon by a constant directional (conservative) step loading P, yielding to a new equilibrium position, defined by $AB\Gamma''\ \Delta''$, the new lengths of the springs are now given by:

$$l_{D1} = h + w_0 \tag{7a}$$

$$l_{D2} = [(a_1 + \upsilon)^2 + (h_2 - w)^2]^{1/2}, l_{D3} = [(a_2 - \upsilon)^2 + (h_2 - w)^2]^{1/2} \tag{7b}$$

and their corresponding translational displacements δ_i can be written as follows

$$\delta_i = l_{Di} - l_i \quad (i = 1, 2, 3) \tag{8}$$

Setting $Q_1 = \upsilon$ and $Q_2 = \mathrm{w}$ as generalized coordinates, using the expressions of the energy functions involved, which are

$$\text{Kinetic energy} \quad K = \tfrac{1}{2} m(\dot{\upsilon}^2 + \dot{w}^2) = \tfrac{1}{2} m(\dot{Q}_1^2 + \dot{Q}_2^2) \tag{9}$$

Total potential energy $V_T = U + \Omega$, with

$$U = \tfrac{1}{2} \sum_{i=1}^{3} K_i \delta_i^2 \text{ and } \Omega = -P(w - w_0) \tag{10}$$

Rayleigh dissipation function

$$F = \tfrac{1}{2} \sum_{i=1}^{3} K_i \dot{\delta}_i^2 \tag{11}$$

introducing the dimensionless quantities

$$\text{dimensionless time} \quad \tau = \sqrt{\frac{K_1}{m}} t$$

$$q_1 = \upsilon/l_a, \quad q_2 = w/l_a, \quad k_2 = K_2/K_1, \quad k_3 = K_3/K_1, \quad c_2 = C_2/\sqrt{K_1 m}, \quad c_3 = C_3/\sqrt{K_1 m}$$

$$\lambda = P/l_a K_1, \quad \bar{l}_{Di} = l_{Di}/l_a \quad (i = 1, 2, 3), \quad \bar{a}_1 = a_1/l_a, \quad \bar{a}_2 = a_2/l_a, \quad \bar{h}_2 = h_2/l_a$$

$$q_{10} = \upsilon_0/l_a, \quad q_{20} = w_0/l_a, \quad \gamma = l_b/l_a \tag{12}$$

and taking also into account the geometric relations

$$\bar{a}_1 = \cos\varphi, \quad \bar{h}_2 = \sin\varphi, \quad \bar{a}_2^2 + \bar{h}_2^2 = \gamma^2 \tag{13}$$

the strongly nonlinear Lagrange differential equations of motion (as in eqn (1)) can be written in dimensionless form as follows:

$$\ddot{q}_1+q_1\left[k_2\left(1-\frac{\beta_2}{\bar{l}_{D2}}\right)+k_3\left(1-\frac{\beta_3}{\bar{l}_{D3}}\right)\right]+k_2\left(1-\frac{\beta_2}{\bar{l}_{D2}}\right)\bar{a}_1-k_3\left(1-\frac{\beta_3}{\bar{l}_{D3}}\right)\bar{a}_2$$
$$+\dot{q}_1\left[c_2\left(\frac{\bar{a}_1+q_1}{\bar{l}_{D2}}\right)^2+c_3\left(\frac{\bar{a}_2-q_1}{\bar{l}_{D3}}\right)^2\right]+\dot{q}_2\left[\frac{-(\bar{a}_1+q_1)}{\bar{l}_{D2}^2}+\frac{(\bar{a}_2-q_2)}{\bar{l}_{D3}^2}\right](\bar{h}_2-q_2)=0 \quad (14)$$

$$\ddot{q}_2+q_2\left[1+k_2\left(1-\frac{\beta_2}{\bar{l}_{D2}}\right)+k_3\left(1-\frac{\beta_3}{\bar{l}_{D3}}\right)\right]-\bar{h}_2\left[k_2\left(1-\frac{\beta_2}{\bar{l}_{D2}}\right)+k_3\left(1-\frac{\beta_3}{\bar{l}_{D3}}\right)\right]-(\lambda+q_{20})$$
$$+\dot{q}_1\left(-c_2\frac{\bar{a}_1+q_1}{\bar{l}_{D2}^2}+c_3\frac{\bar{a}_2-q_1}{\bar{l}_{D3}^2}\right)(\bar{h}_2-q_2)+\dot{q}_2\left[c_1+\left(\frac{c_2}{\bar{l}_{D2}^2}+\frac{c_3}{\bar{l}_{D3}^2}\right)(\bar{h}_2-q_2)^2\right]=0 \quad (15)$$

subject to initial conditions

$$q_1(0)=q_{10},\quad q_2(0)=q_{20},\quad \dot{q}_1(0)=\dot{q}_2(0)=0. \quad (16)$$

Eliminating the inertia terms from eqns (14) and (15), we obtain to the nondimensionalized static equilibrium equations of the foregoing system, given by

$$\frac{\partial V_T}{\partial q_1}=k_2\left(1-\frac{\beta_2}{\bar{l}_{D2}}\right)(\bar{a}_1+q_1)-k_3\left(1-\frac{\beta_3}{\bar{l}_{D3}}\right)(\bar{a}_2-q_1)=0$$
$$\frac{\partial V_T}{\partial q_2}=(q_2-q_{20})-\left[k_2\left(1-\frac{\beta_2}{\bar{l}_{D2}}\right)+k_3\left(1-\frac{\beta_3}{\bar{l}_{D3}}\right)\right](\bar{h}_2-q_2)-\lambda=0 \quad (17)$$

while the corresponding total potential energy function equals to

$$V_T=\frac{1}{2}(q_2-q_{20})^2+\frac{1}{2}\sum_{j=2}^{3}(\bar{l}_{Dj}-\beta_j)^2-\lambda(q_2-q_{20}) \quad (18)$$

4. Numerical results and discussion

Let us consider at first the case of an asymmetrical roof model with $\gamma=1.50$, $\varphi=20^\circ$, $k_2=20$, $k_3=18$. The physical equilibrium paths (λ vs q_i) shown in Fig. 2 (while there are no complementary equilibrium configurations) reveal a limit point system, for which the simultaneous solution of eqns (17) and $V_T=0$ from relation (18) enables us to establish the value of the approximate dynamic buckling load $\tilde{\lambda}_D=0.29571902$, being a lower bound of the exact one $\lambda_D=0.295731880$ (for zero damping). The latter is obtained numerically using the criterion, which requires the motion to touch the postbuckling 'unstable' path. For $\lambda=\tilde{\lambda}_D$ of course, there exists no escape passage (since $V_T=0$ constitutes a repeller barrier) and the basins of attraction of the two stable fixed points corresponding to this specific loading value are simply tangent at point D. This can be observed from the $V_T=0$ contour on the q_1q_2 plane of the energy surface shown in Fig. 3, where E and E' are the two stable equilibria mentioned above. From this illustration one can clearly perceive the difference in dimensions between the two domains, with the one belonging to E' being quite smaller. Furthermore, for $\lambda=\lambda_D$ dynamic buckling occurs in the vicinity of a saddle

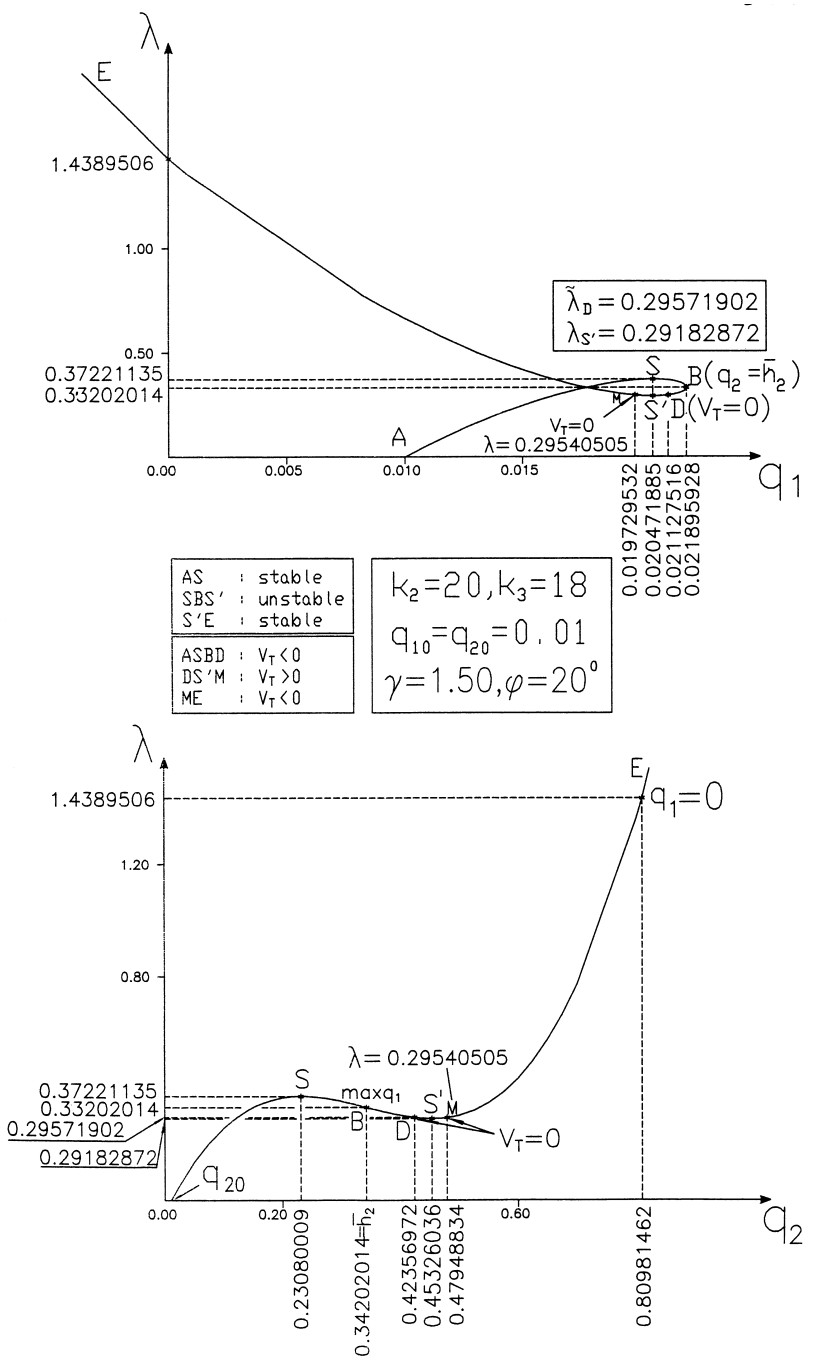

Fig. 2. Physical equilibrium paths (q_i, λ $i = 1, 2$) for a roof model with $q_{10} = q_{20} = 0.01$, $\gamma = 1.50$, $\varphi = 20^\circ$ and $k_2 = 20$, $k_3 = 18$ (case 1).

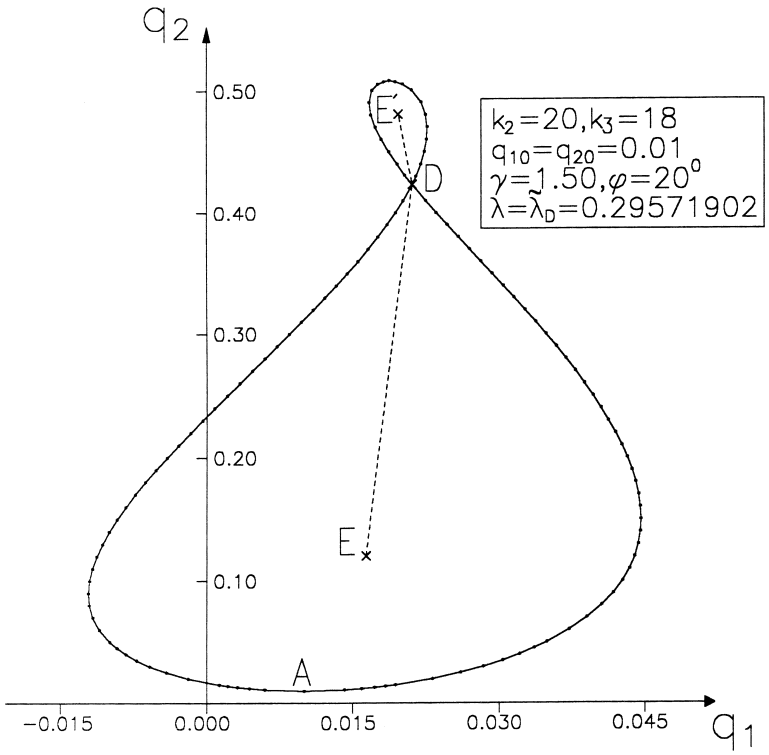

Fig. 3. Contour $V_T = 0$ on the q_1q_2 plane of model case 1 for $\lambda = \tilde{\lambda}_D$.

and the motion (starting at A) is for zero damping, as expected, lead from one basin to the other; these basins form a two-well surface, as shown in the $V_T = 0$ contour plot of Fig. 4, where also the corresponding motion projection is depicted, while the energy surface itself and various contours on base are presented in Fig. 5, from where it is obvious that $|V_T|_{E_{S1}} > |V_T|_{E_{S2}}$; this implies that the basin of attraction of the prebuckling stable fixed point is not only longer and wider, but also deeper than the one of the postbuckling stable equilibrium. If damping is accounted for, introducing $c_1 = 0.02$, $c_2 = 0.05$ and $c_3 = 0.04$ the dynamic buckling load λ_{DD} is found to be equal to 0.29704878 (following the same procedure as the one used for λ_D). The motion, projection of which on the q_1q_2 plane is presented in Fig. 6, starting at A passes through the escape passage near the saddle point DD and is captured by E', where it finally settles, as shown in the phase plane portraits (q_i, $\dot{q}_i$ $i = 1, 2$) of Fig. 8, while the total potential energy surface for $\lambda = \lambda_{DD}$ is presented in Fig. 7. This last surface representation, compared to the one of Fig. 5, implies that as λ increases, the domain of the (natural) postbuckling stable fixed point gets deeper and larger. The aforementioned effect (of increasing λ) can also be observed in the zero potential surface of Fig. 9, valid for $\lambda = 0.33$.

For $\lambda > \lambda_{DD}$ according to previous analyses one would expect a similar dynamic response of point attractor type on the remote stable equilibrium. But this is not the case for the system under consideration, since, as shown in Fig. 10, for $\lambda = 0.32$ although the dynamic buckling mechanism has already occurred through the vicinity of a saddle, the motion comes back and forth from one

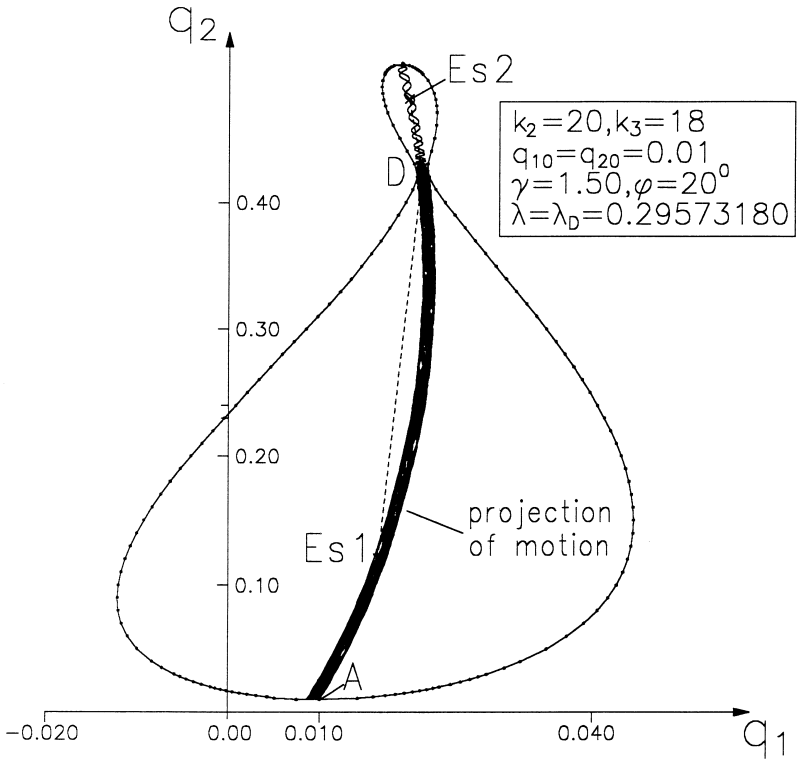

Fig. 4. Contour $V_T = 0$ and motion projection on the q_1q_2 plane of model case 1 for $\lambda = \lambda_D$.

domain to the other and is finally attracted by the prebuckling stable fixed point. On the contrary, for $\lambda = 0.33$ and $\lambda = 0.35$ the system moves in a similar manner, to be finally attracted by the postbuckling stable equilibrium, as shown in the phase plane portraits of Figs. 11 and 12 respectively. This new finding, described above, can be reached only via a fully nonlinear (global) dynamic analysis, specifying that after dynamic buckling some but not all statically stable equilibria of the natural postbuckling path, for limit point systems, are dynamically locally stable and globally unstable, while others are simultaneously locally and globally asymptotically stable, like the ones for $\lambda < \lambda_{DD}$, i.e. before dynamic buckling.

A case of equal interest and importance is the one dealt with below, associated with a roof model with the following characteristic properties: $q_{10} = q_{20} = 001$, $k_2 = 1.00$, $k_3 = 0.80$ and $\varphi = 60^\circ$. The physical equilibrium paths obtained from eqn (17) for $\gamma = 1.00$, 1.50, 2.00 and presented in Fig. 13, possess the special attribute that all along these paths the total potential energy is negative definite. Systems for $\gamma > 1.00$ (asymmetric roofs) will not be considered further, since from the shape of their equilibrium paths their dynamic response is totally predictable. On the other hand, for the symmetric roof model of the foregoing case ($\gamma = 1.00$), which is a limit point like one, eqn (17) yields two complementary equilibrium configurations, depicted in Fig. 14. For $\lambda_S > \lambda > \lambda'_S$ it is profound that multiple stable fixed points, close to each other, correspond to the same amount of loading; in the sequel their domains may form a highly irregular energy surface with numerous

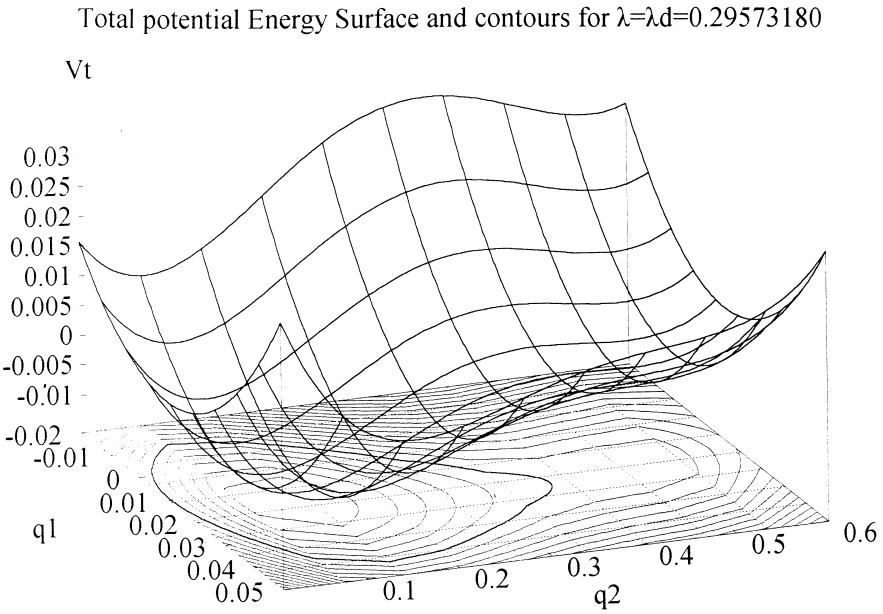

Fig. 5. Total potential energy surface and contours of model case 1 for $\lambda = \lambda_D$.

local maxima and minima, a fact offering to the undamped motion more than one possible direction—escape passages. In this manner the system could move following a complicated pattern, from one basin to the other. This indeed happens for the system under study, as clearly shown throughout Figs 15–18, where the zero potential contours and motion projections as well as energy surfaces are presented, for certain characteristic loading levels.

The questions immediately arising are what will the nature of the system's dynamic response be if damping is accounted for and is this response affected or not by the amount of dissipation considered. These are clarified examining the dynamic behavior of the foregoing model for $\lambda = 0.80$, $c_1 = c_2 = 0.01$, $c_3 = 0.008$. It is found that the mechanism of dynamic buckling (near a saddle) is valid, a large amplitude motion is initiated, leading the system through the escape passage back and forth (from domain to domain), to be finally attracted by the pre-buckling stable natural fixed point. If again, for the same loading, damping is doubled the system exhibits a point attractor response in the large. This is clearly shown in the phase plane portraits of Figs 20 and 22 and the projection of motion on the q_1q_2 plane depicted in Figs 19 and 21 respectively. In this case although four complementary equilibria exist, they do not affect the damped motion, which nevertheless is more 'wandering' than in usual cases. For higher levels of the loading the system behaves dynamically in a different pattern. For instance, if we consider the case of $\lambda = 0.90$ (associated with six complementary equilibria) the system's motion may or may not 'visit' the domains of all stable equilibria. This depends on the amount of dissipation, since for $c_1 = c_2 = 0.01$, $c_3 = 0.008$ the motion after passing through all domains is finally attracted by the remote stable natural equilibrium, while for double damping the system's behavior is similar to the one for $\lambda = 0.80$ (for the

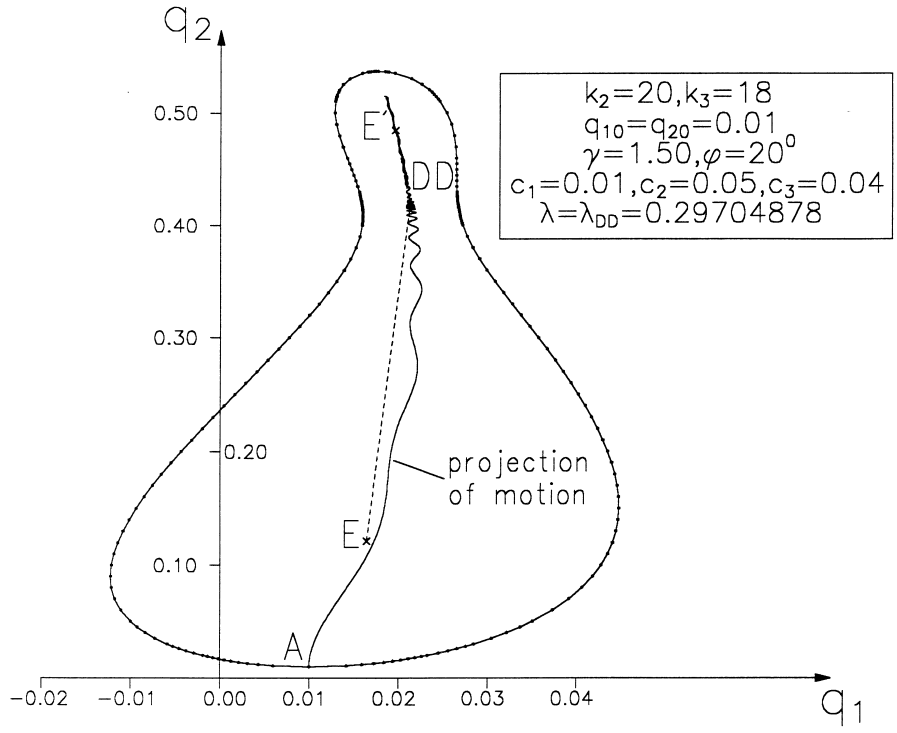

Fig. 6. Contour $V_T = 0$ and damped motion projection on the q_1q_2 plane of model case 1 with $c_1 = 0.01$, $c_2 = 0.05$, $c_3 = 0.04$, and $\lambda = \lambda_{DD}$.

same damping). All these are presented graphically in Figs 24 and 25, while the energy surface for $\lambda = 0.90$, being as expected quite complicated, is shown in Fig. 23.

5. Conclusions

The most important conclusions drawn from this study are the following:

1. Dynamic buckling of autonomous potential dissipative systems of a classical limit point type is not always associated either with a point attractor response on a remote stable equilibrium or an unbounded motion. Under certain conditions and although dynamic buckling has already occurred, the escaped motion returns through the vicinity of the saddle and is finally attracted by the stable fixed point belonging to the physical prebuckling stable (primary) equilibrium path. This new phenomenon is captured only via a straightforward nonlinear global dynamic analysis revealing for some fixed points simultaneous local and global dynamic stability after dynamic buckling.
2. This third possibility of postbuckling dynamic response leads to the significant remark, that from a qualitative point of view the geometry and surface structure of both pre- and postbuckling domains must be accounted for, in conjunction with other parameters.

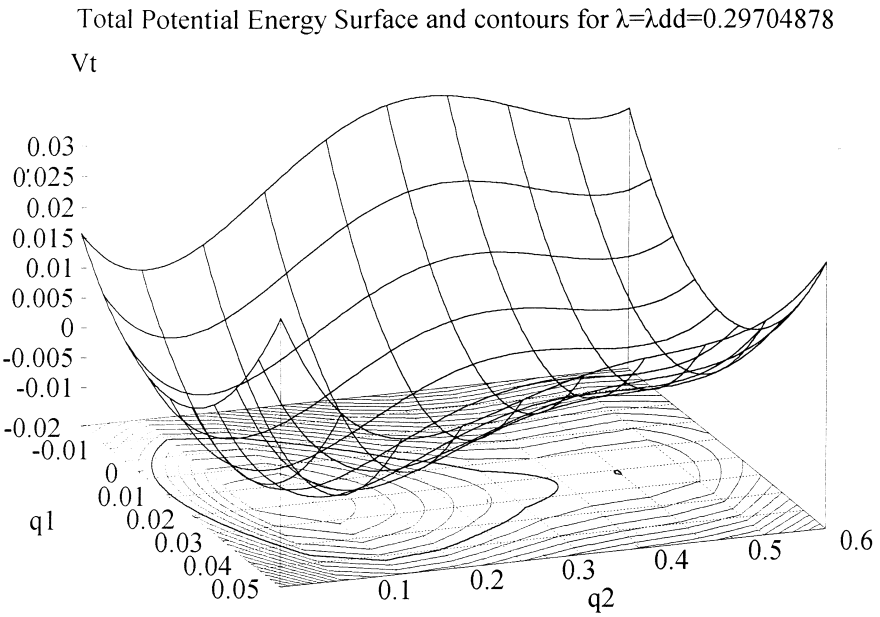

Fig. 7. Total potential energy surface and contours of model case 1 for $\lambda = \lambda_{DD}$.

3. The phenomenon described above may also occur for limit point like systems, whose physical equilibrium path possesses always negative total potential. Such systems exhibit various complementary equilibrium configurations, and for loads higher than a certain level the total potential energy surface contains numerous domains, becoming quite irregular and complicated. Depending on the number of stable complementary equilibria corresponding to the same loading, the system's motion may enter these domains, until it is finally attracted by always physical equilibriia, either pre- or postbuckling. In this case the surface structure of all basins of attraction must be considered, while the only way to establish the overall response is once again to perform a fully nonlinear dynamic analysis, since energy criteria are no longer applicable, due to negative potential.
4. All the above are verified through the dynamic stability analysis of a 2-D.O.F. autonomous potential system, simulating an everyday practice real structure, an asymmetrical suspended roof.

Acknowledgments

The author wishes to express his gratitude to Prof. G.T. Michaltsos at NTUA for his encouragement and Prof. Alex. Vakakis of University of Illinois at Urbana Champaign for his valuable suggestions.

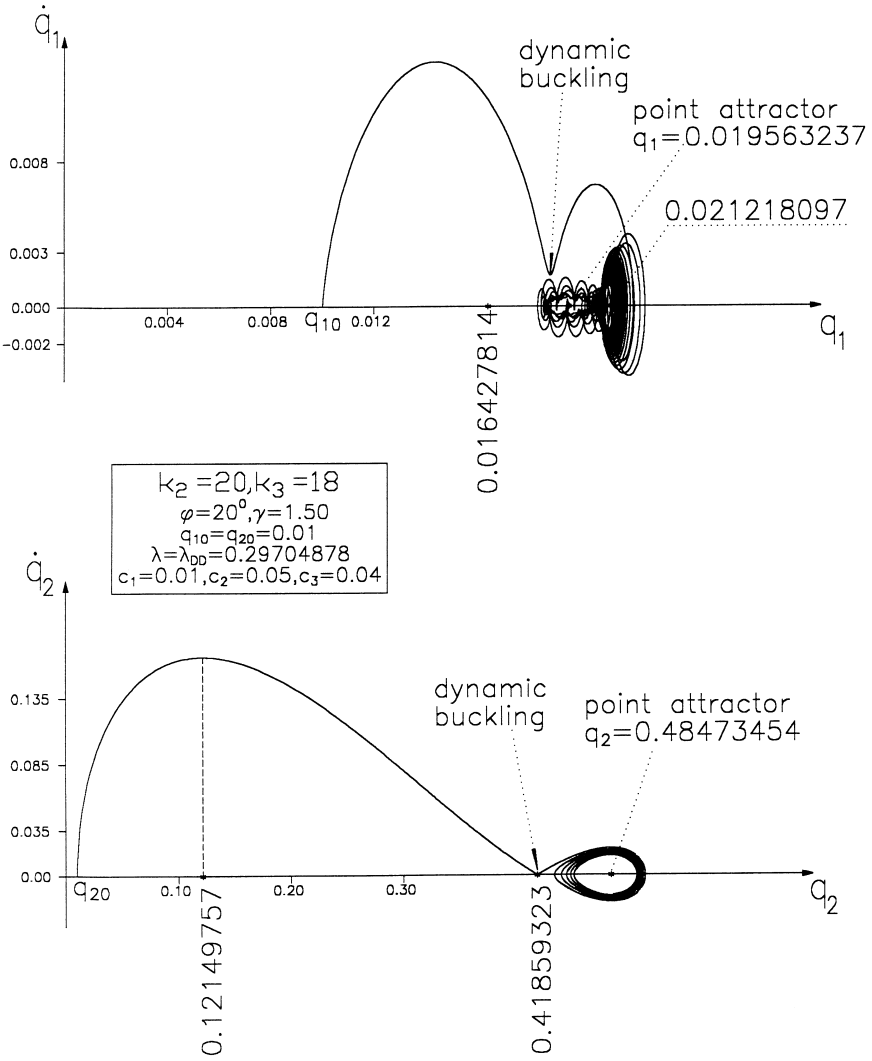

Fig. 8. Phase plane portraits (q_i, $\dot{q}_i$ $i = 1, 2$) of model case 1 with $c_1 = 0.01$, $c_2 = 0.05$, $c_3 = 0.04$ and $\lambda = \lambda_{DD}$, revealing a point attractor in the large (remote stable equilibrium).

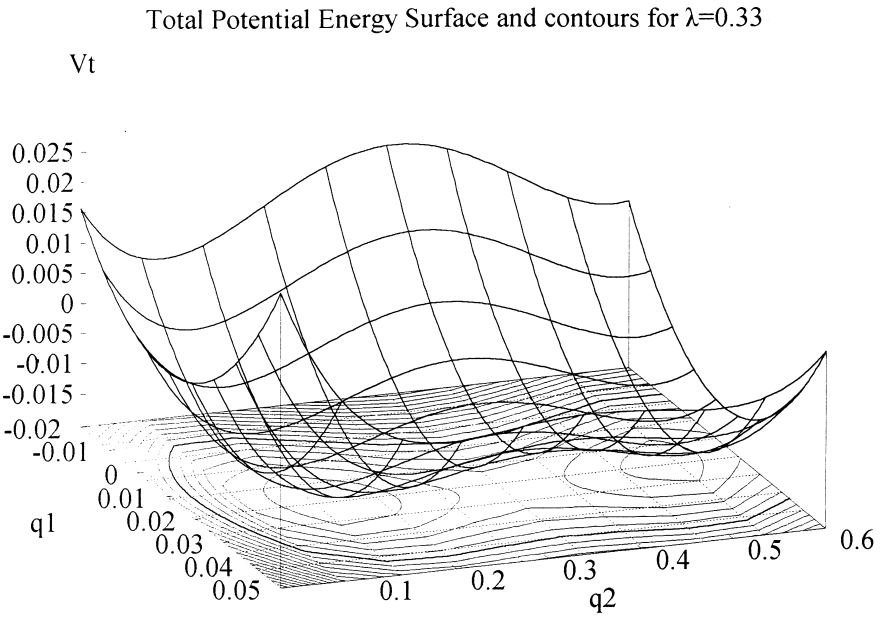

Fig. 9. Total potential energy surface of model case 1 for $\lambda = 0.33$.

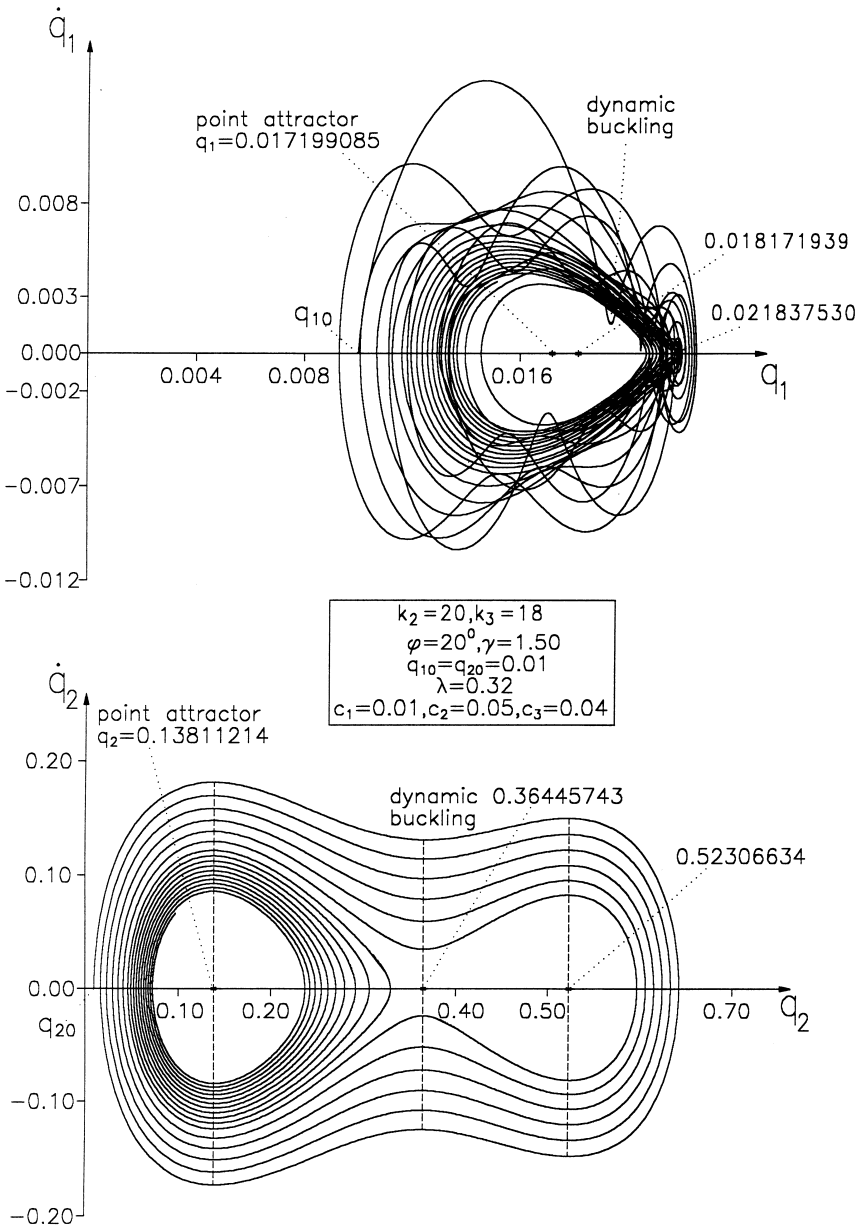

Fig. 10. Phase plane portraits (q_i, $\dot{q}_i$ $i = 1, 2$) of model case 1 with $c_1 = 0.01$, $c_2 = 0.05$, $c_3 = 0.04$ and $\lambda = 0.32$, showing a point attractor on the prebuckling stable fixed point.

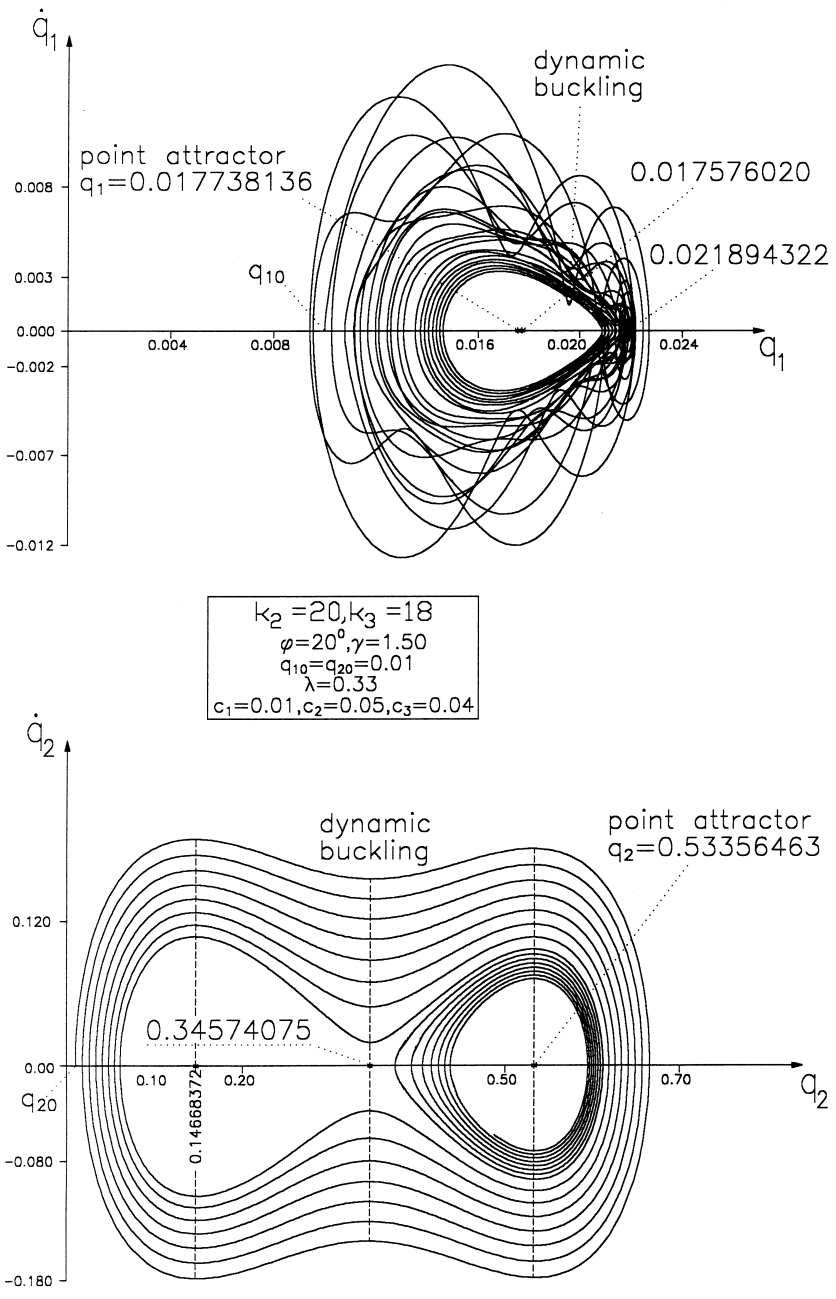

Fig. 11. Phase plane portraits (q_i, $\dot{q}_i$ $i = 1, 2$) of model case 1 with $c_1 = 0.01$, $c_2 = 0.05$, $c_3 = 0.04$ and $\lambda = 0.33$, showing a point attractor in the large (remote stable equilibrium).

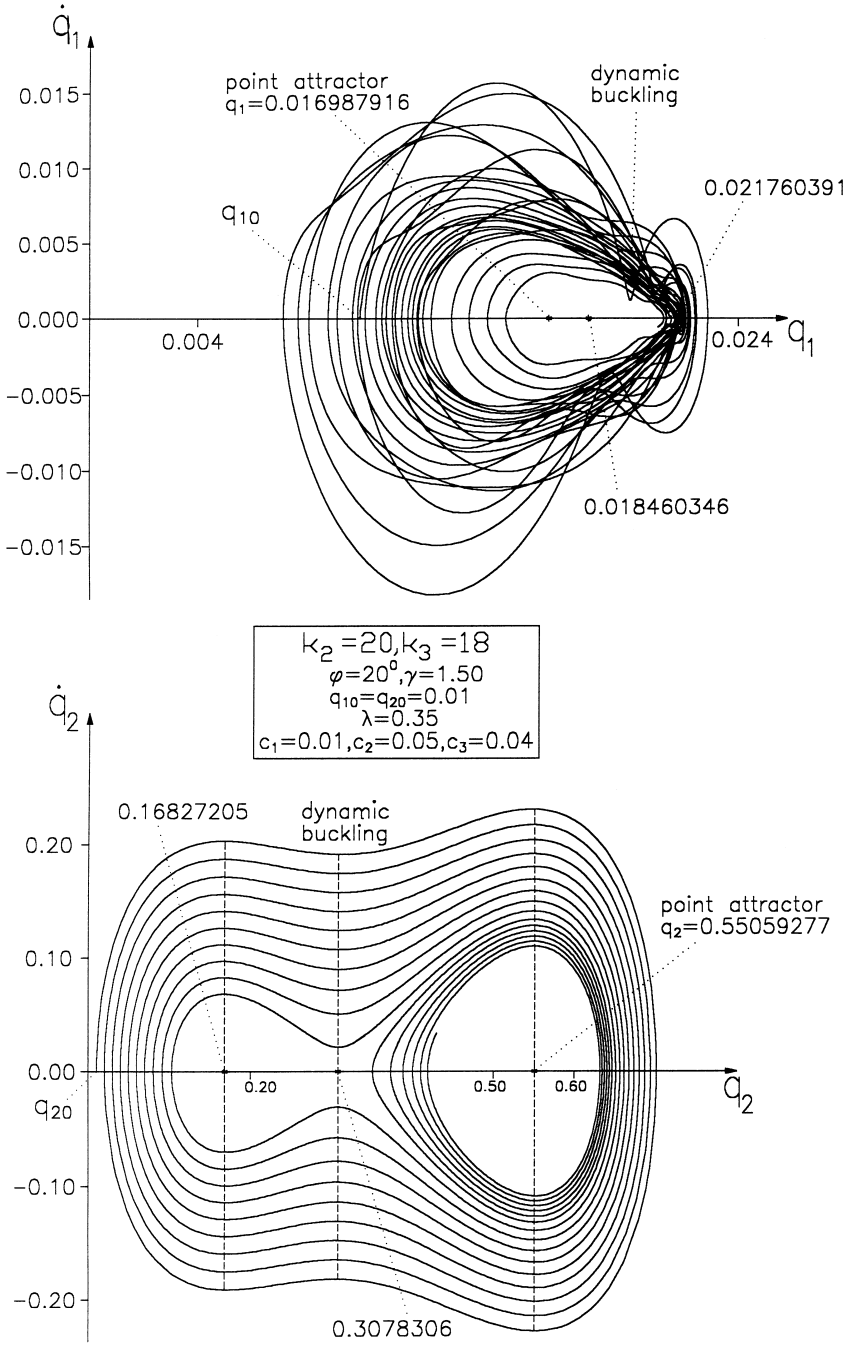

Fig. 12. Phase plane portraits (q_i, $\dot{q}_i$ $i = 1, 2$) of model case 1 with $c_1 = 0.01$, $c_2 = 0.05$, $c_3 = 0.04$ and $\lambda = 0.35$, showing a point attractor in the large (remote stable equilibrium).

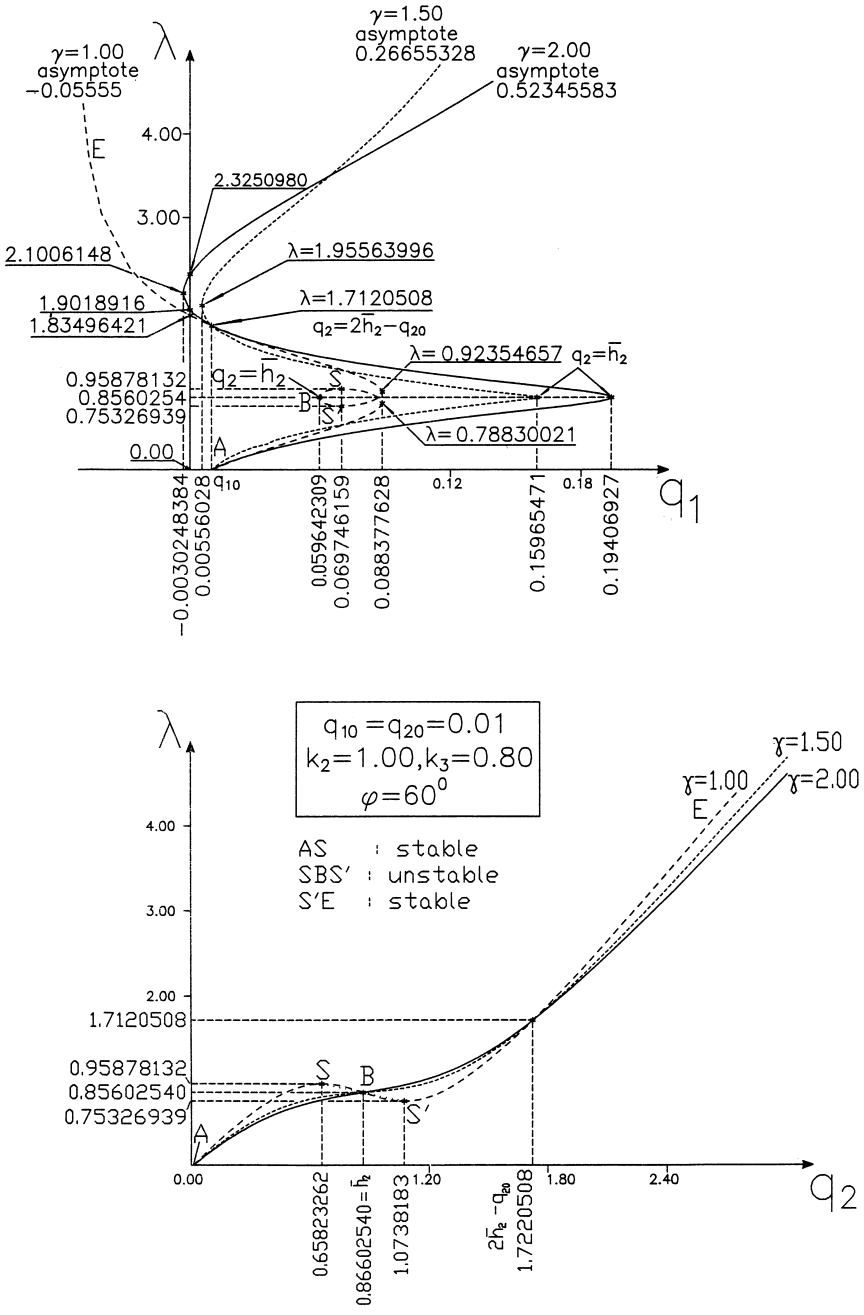

Fig. 13. Physical equilibrium paths (q_i, $\lambda i = 1, 2$) for a roof model with $q_{10} = q_{20} = 0.01$, $k_2 = 1.00$, $k_3 = 0.80$, $\varphi = 60^\circ$ and three values of the asymmetry parameter γ (1, 1.50, 2).

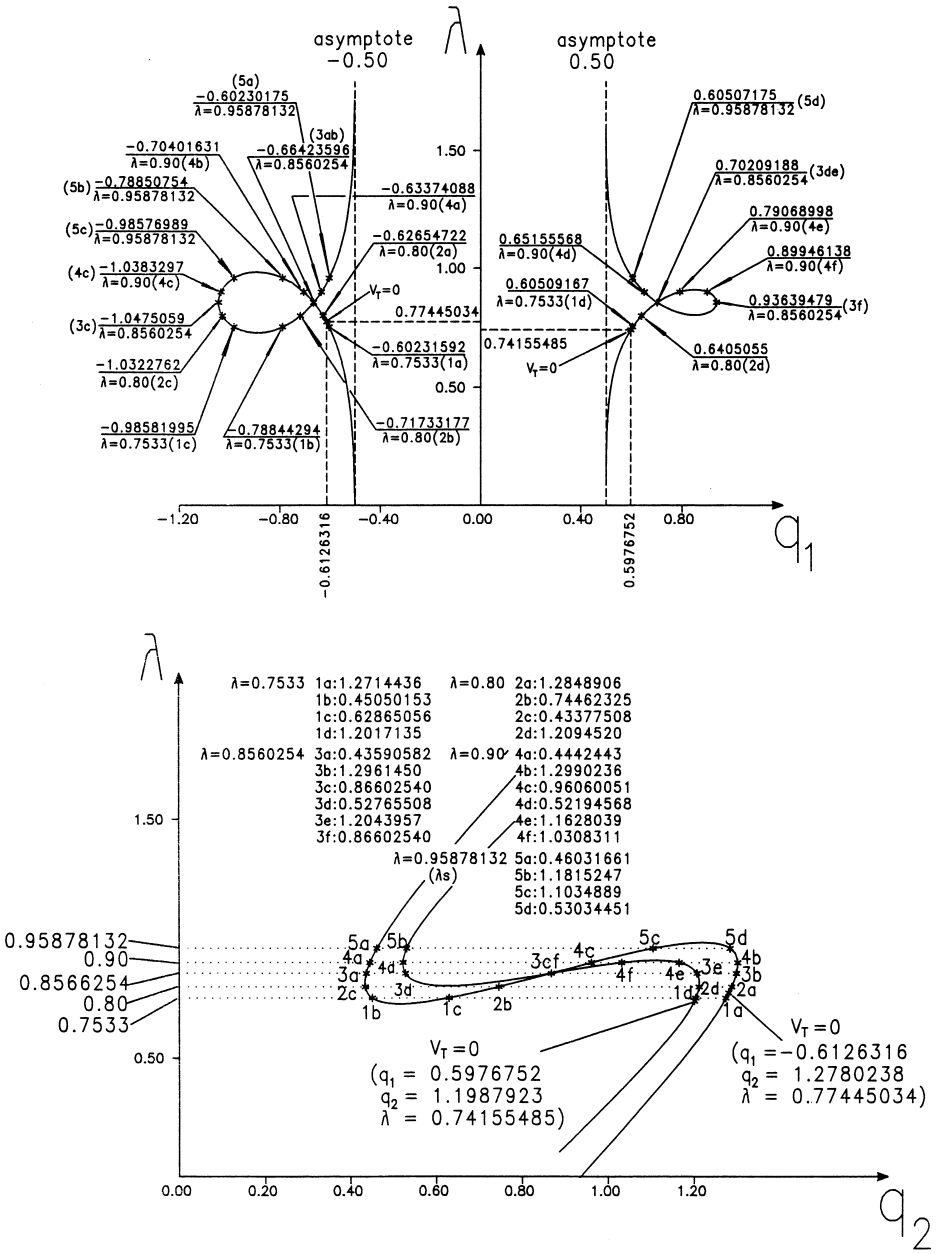

Fig. 14. Complementary (physically not accepted) equilibrium paths (q_i, λ) for a roof model with $q_{10} = q_{20} = 0.01$, $k_2 = 1.00$, $k_3 = 0.80$, $\varphi = 60^\circ$ and $\gamma = 1.00$ (case 2).

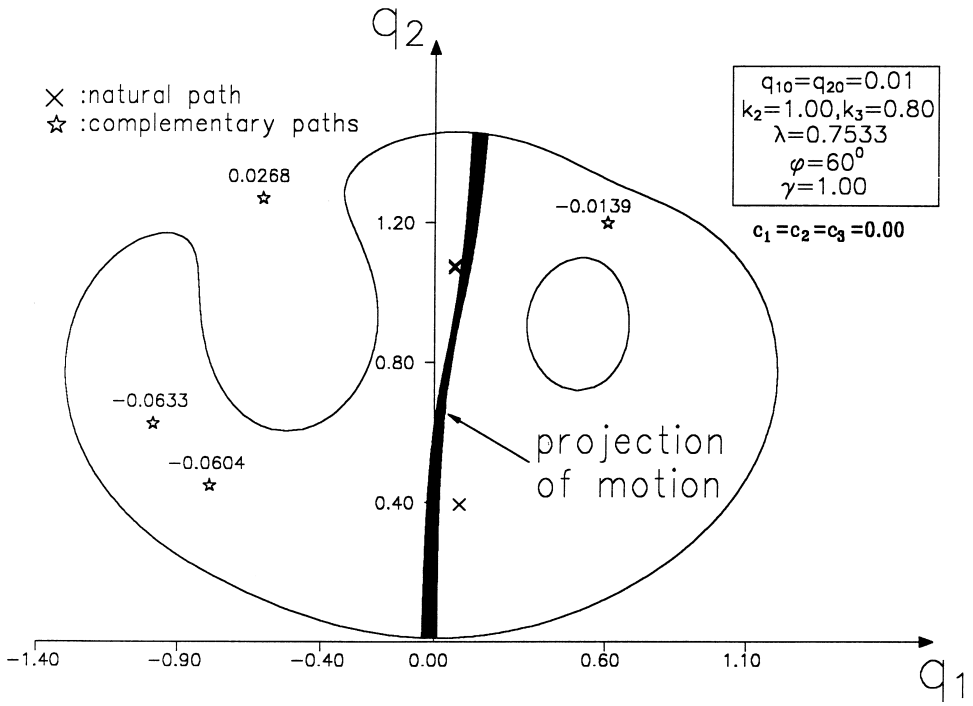

Fig. 15. Contour $V_T = 0$ and undamped motion projection on the q_1q_2 plane of model case 2 for $\lambda = 0.7533$.

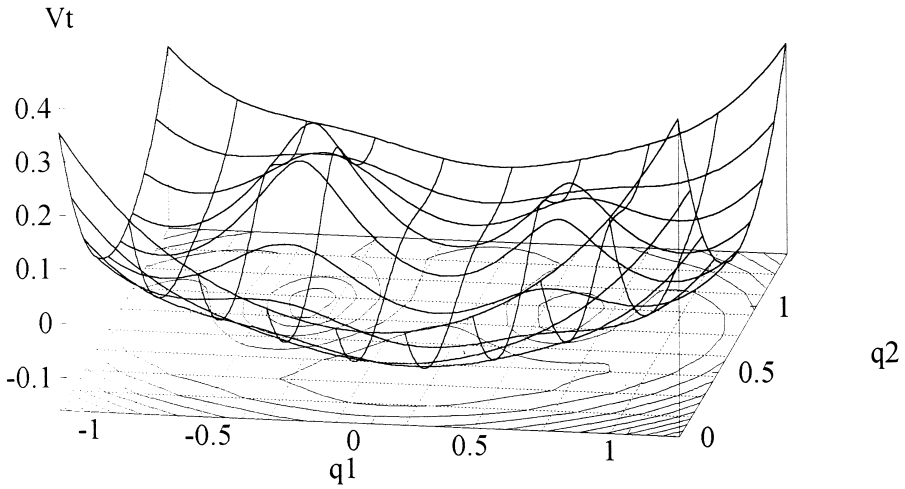

Fig. 16. Total potential energy surface and contours of model case 2 for $\lambda = 0.7533$.

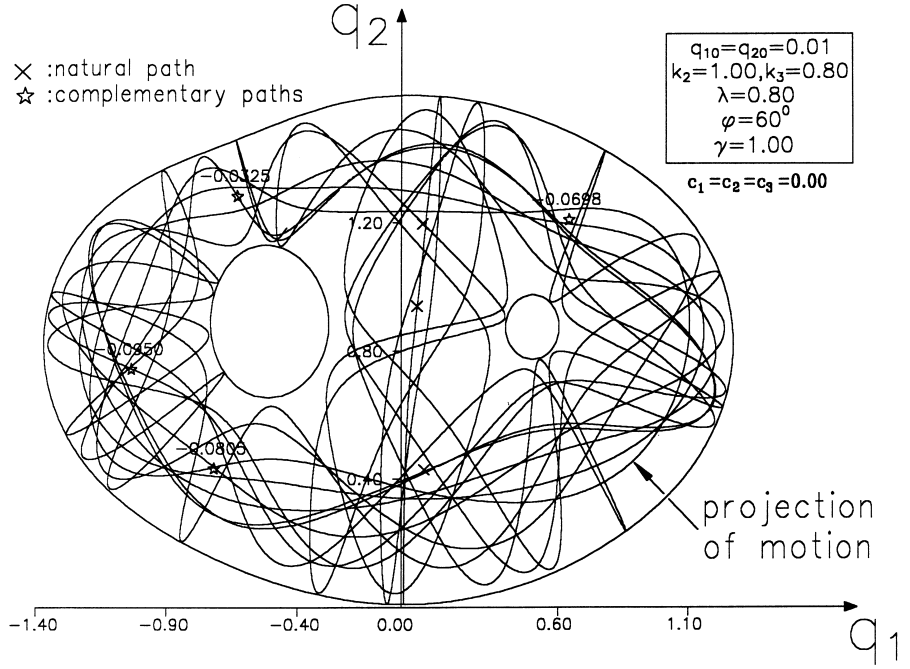

Fig. 17. Contour $V_T = 0$ and undamped motion projection on the q_1q_2 plane of model case 2 for $\lambda = 0.80$.

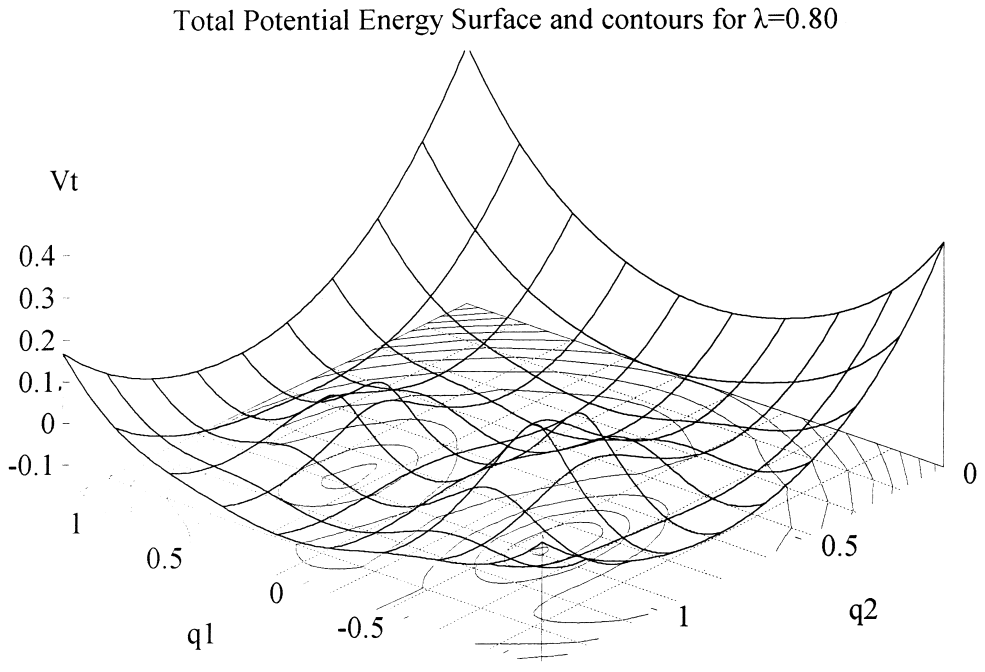

Fig. 18. Total potential energy surface and contours of model case 2 for $\lambda = 0.80$.

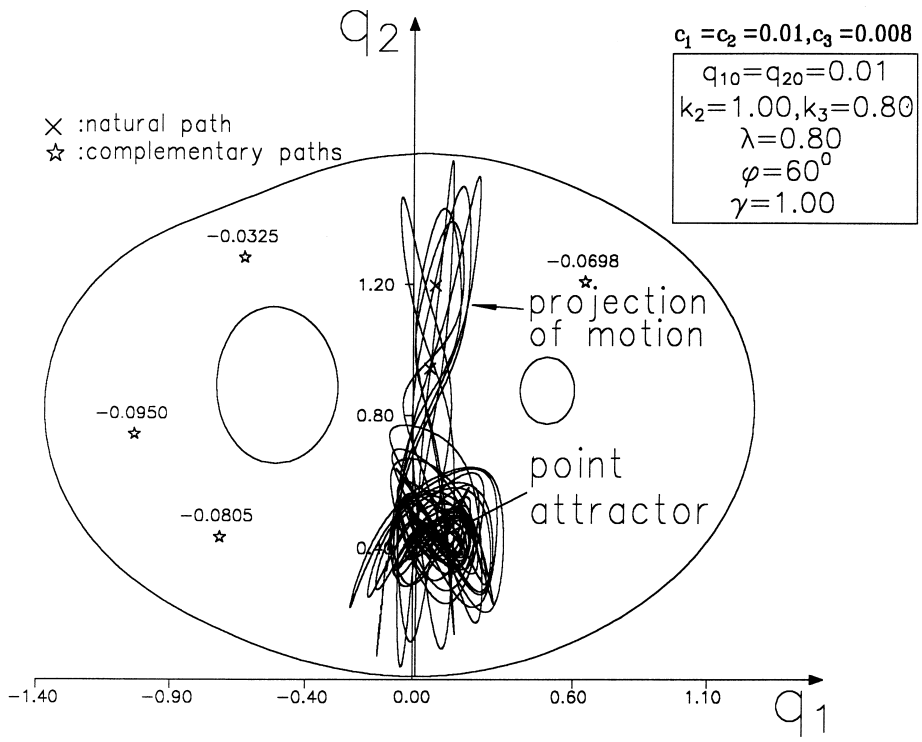

Fig. 19. Contour $V_T = 0$ and undamped motion projection on the ($c_1 = c_2 = 0.01$, $c_3 = 0.008$) of model case 2 for $\lambda = 0.80$ (point attractor at the prebuckling stable equilibrium).

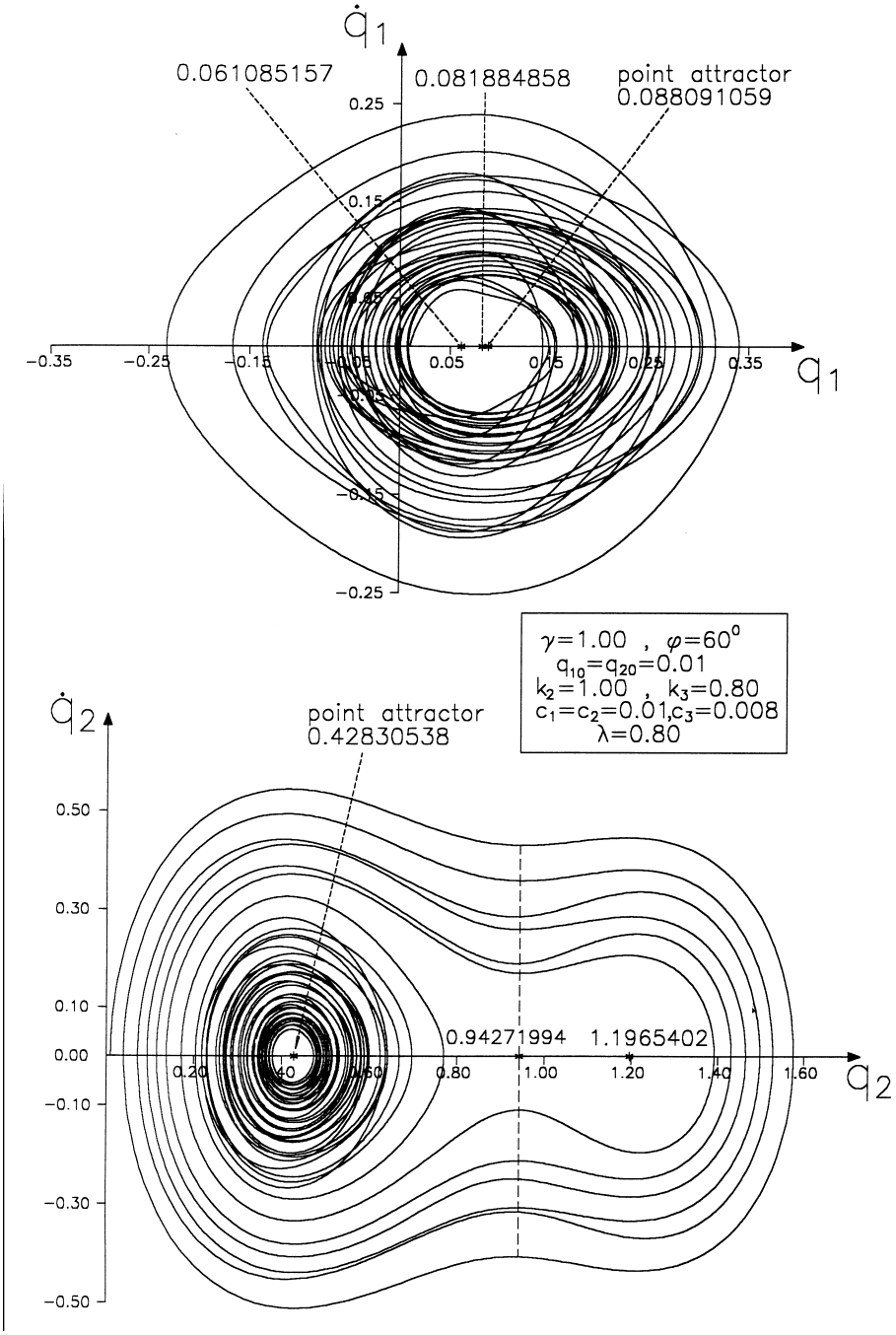

Fig. 20. Phase plane portraits (q_i, $\dot{q}_i$ $i = 1, 2$) of the damped motion shown in Fig. 19.

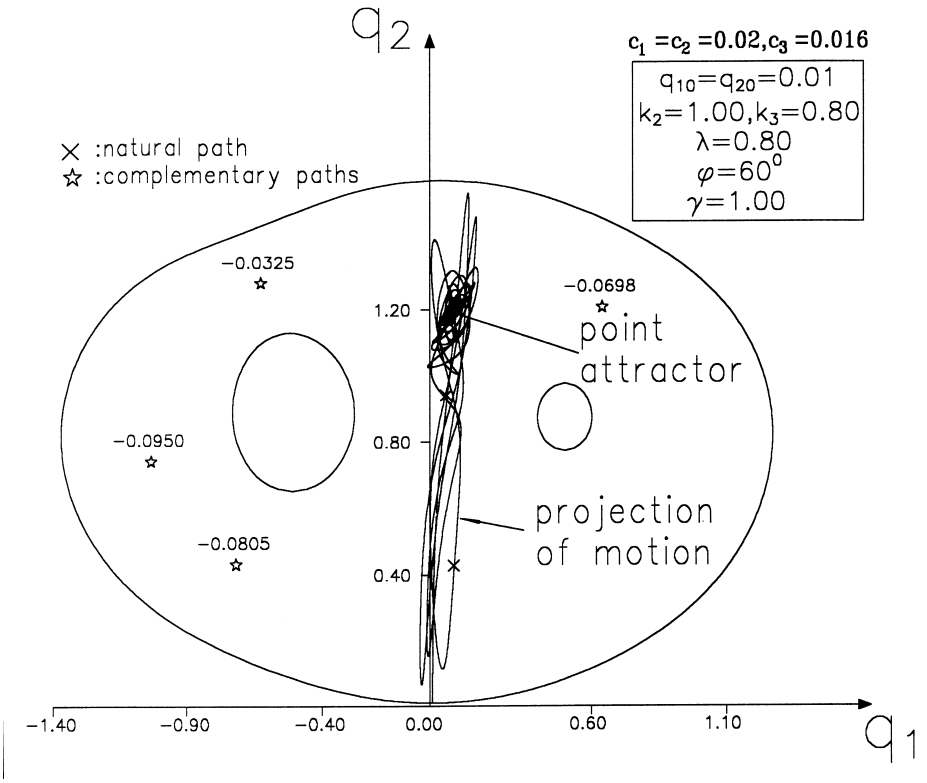

Fig. 21. Contour $V_T = 0$ and damped motion projection ($c_1 = c_2 = 0.02$, $c_3 = 0.016$) of model case 2 for $\lambda = 0.80$ (remote attractor).

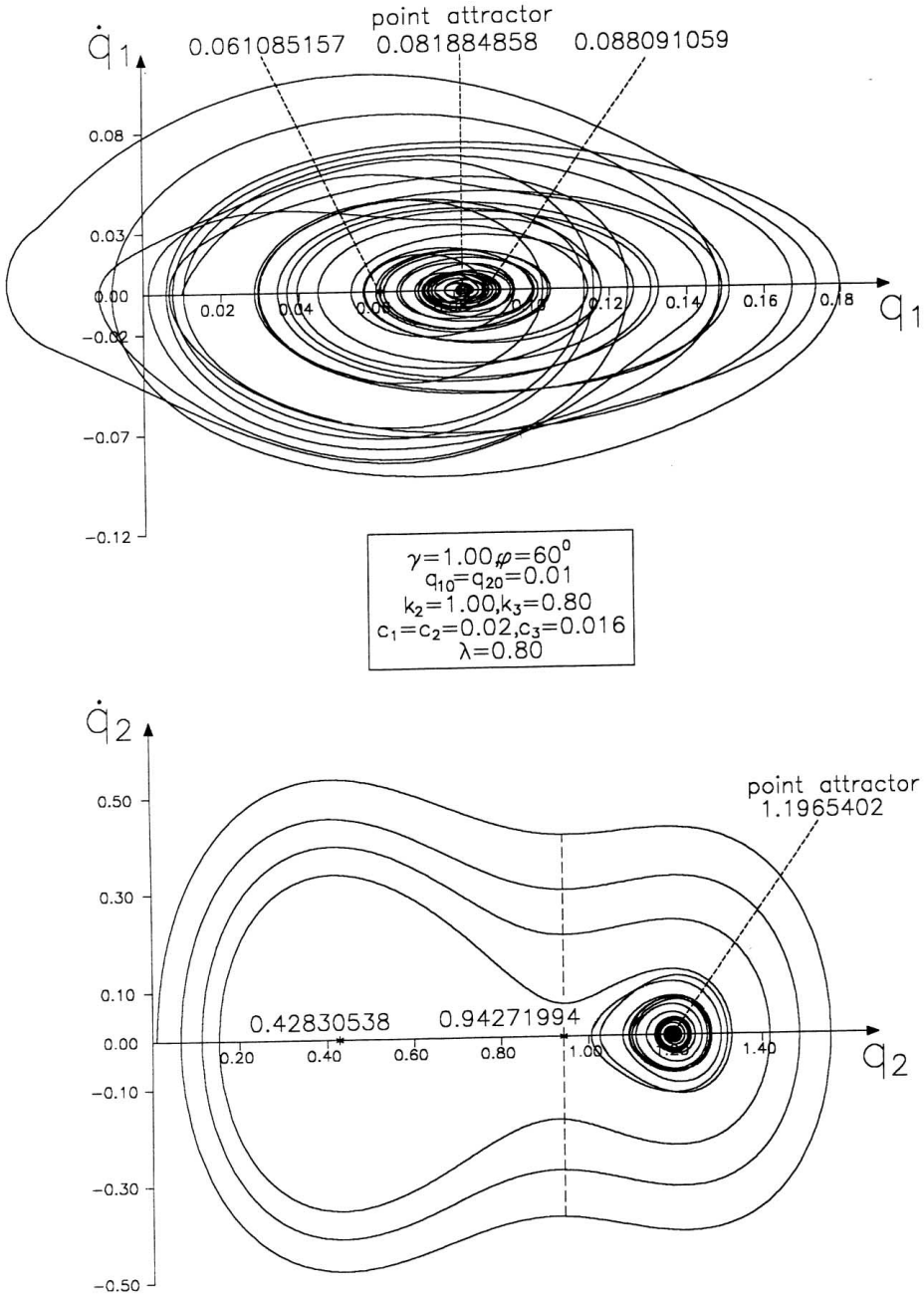

Fig. 22. Phase plane portraits (q_i, $\dot{q}_i$ $i = 1, 2$) of the damped motion shown in Fig. 21.

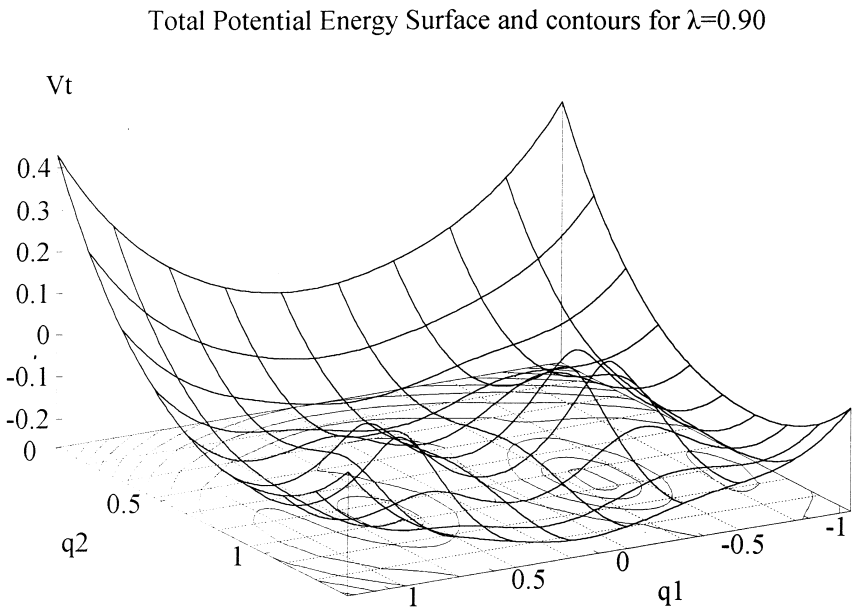

Fig. 23. Total potential energy surface and contours of model case 2 for $\lambda = 0.90$.

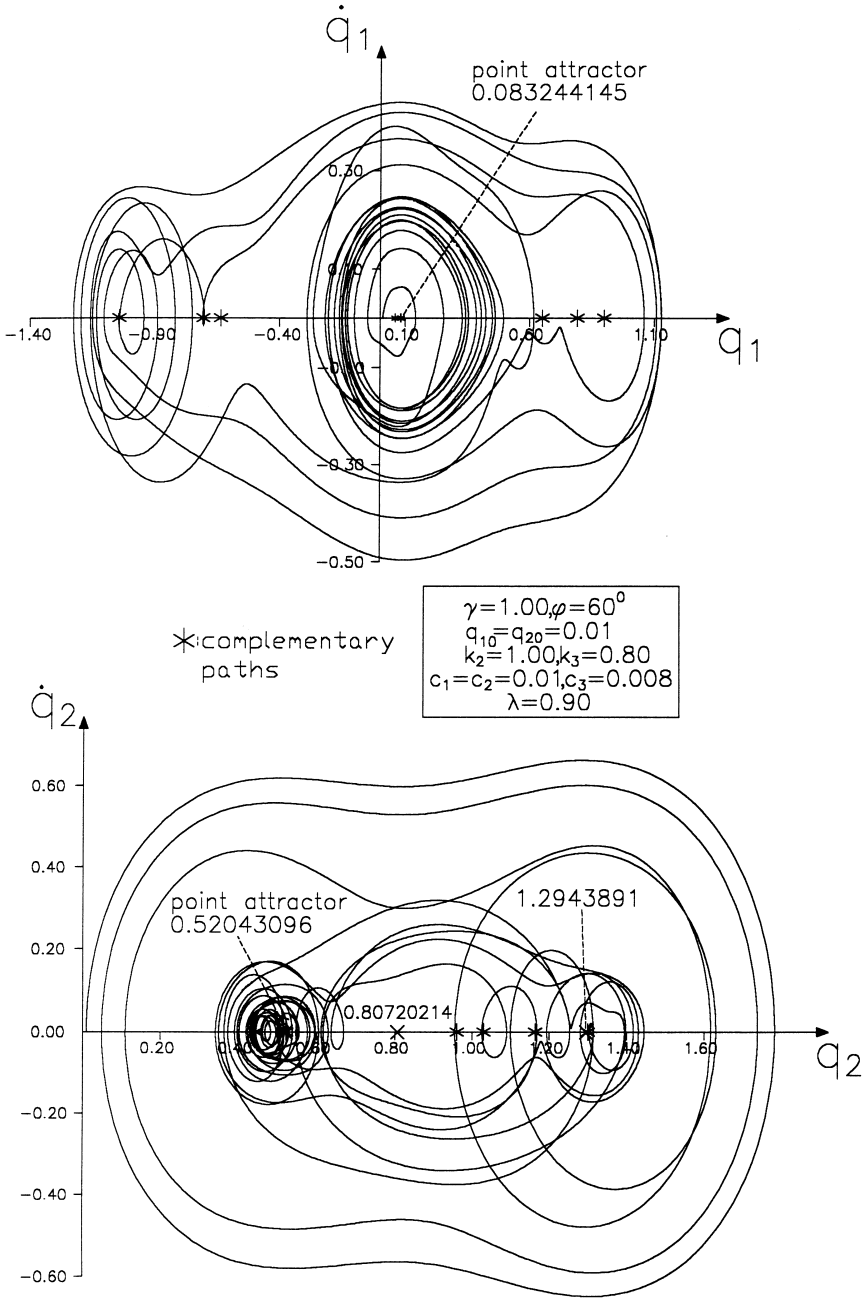

Fig. 24. Phase plane portraits (q_i, $\dot{q}_i$ $i = 1, 2$) for model case 2, with $c_1 = c_2 = 0.01$, $c_3 = 0.008$ and $\lambda = 0.90$, revealing a point attractor on the prebuckling stable equilibrium, after approaching all complementary fixed points.

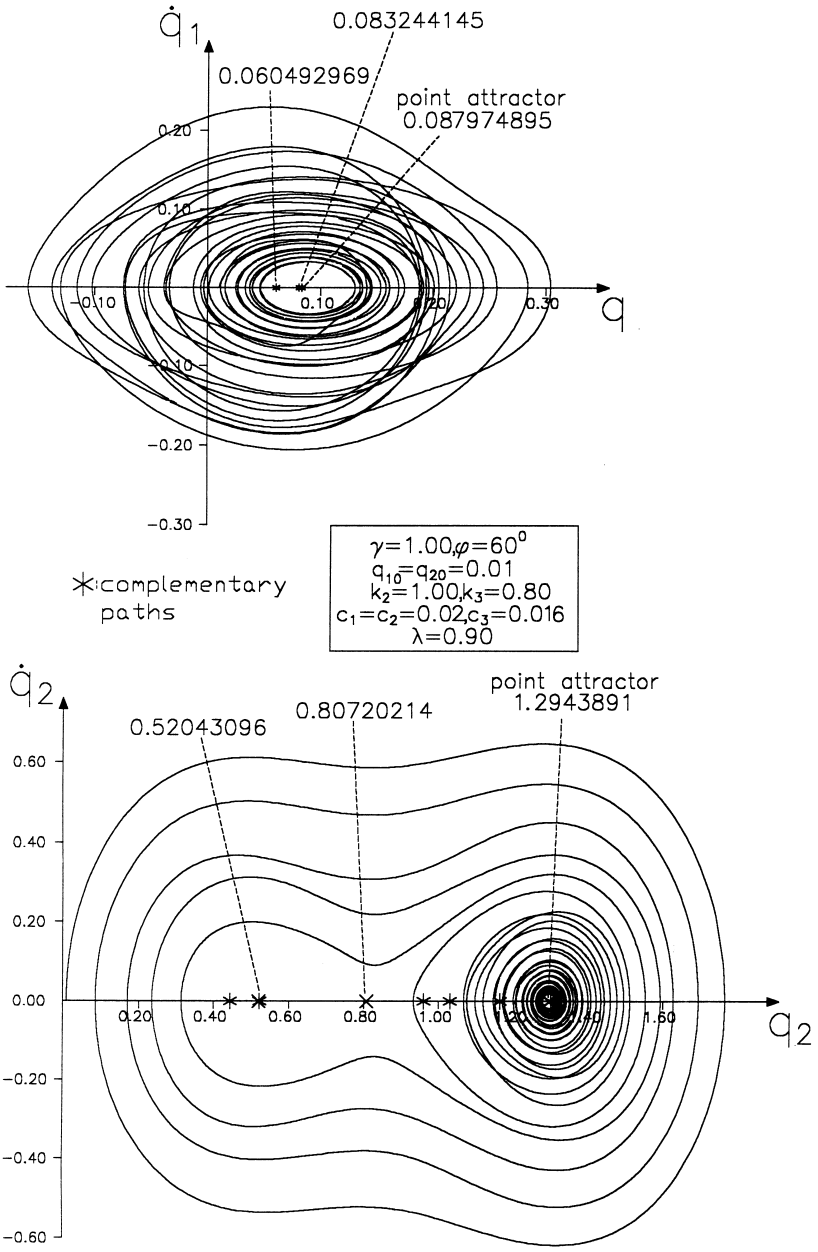

Fig. 25. Phase plane portraits (q_i, $\dot{q}_i$ $i = 1, 2$) for model case 2, with $c_1 = c_2 = 0.02$, $c_3 = 0.016$ and $\lambda = 0.90$, showing a point attractor in the large, ignoring complementary equilibria.

References

Dubrovin, B.A., Fomenko, A.T., Novikov, S.P., 1984. Modern Geometry-Methods and Applications, Part I. The Geometry of Surfaces, Transformation Groups and Fields, Springer-Verlag, New York, Heidelberg, Berlin.

Dubrovin, B.A., Fomenko, A.T., Novikov, S.P., 1984. Modern Geometry-Methods and Applications, Part II. The Geometry and Topology of Manifolds, Springer-Verlag, New York, Heidelberg, Berlin.

Gantes, Ch., Kounadis, A.N., 1995. Energy-based dynamic buckling estimates of autonomous dissipative systems. AIAA J. 33 (7), 1342.

Guckenheimer, J., Holmes, D.J., 1983. Nonlinear Oscillations, Dynamical Systems and Bifurcations of Vector Fields, Springer-Verlag, New York, Heidelberg, Berlin.

Huseyin, K., 1981. On the Stability of Equilibrium Paths Associated with Autonomous Systems. Journal of Applied Mechanics 48, 183–187.

Kounadis, A.N., 1993a. Criteria and estimates in the nonlinear dynamic buckling of dissipative/nondissipative structural systems under step load. Potential Systems. CISM Course on Nonlinear Stability of Structures, Udine, Italy, 6–20 Sept. (Eds.). Kounadis A.N. Krätzig, W.B. Lecture Notes by Springer-Verlag, Vol. I, 74–142.

Kounadis, A.N., 1993. Static and dynamic, local and global, bifurcations in nonlinear autonomous (damped or undamped) structural systems. AIAA J. 31 (8), 1468–1477.

Kounadis, A.N., 1993. Nonlinear Dynamic Buckling and Stability of Autonomous Structural Systems. Int. J. Mech. Sci. 35 (8), 643–656.

Kounadis, A.N., 1994. A qualitative analysis for the local and global dynamic buckling and stability of autonomous discrete systems. Q. J. Appl. Math. 47 (2), 269–295.

Kounadis, A.N., 1996. Qualitative Criteria in Non-Linear Dynamic Buckling and Stability of Autonomous Dissipative Systems. Int. J. Non-Linear Mechanics 31 (6), 887–906.

Lebovitz, N.R., Schaar, R.J., 1975. Exchange of stabilities in autonomous systems. Stud. Appl. Math. 54, 229–260.

Michaltsos, G.T., Sophianopoulos, D.S., 1998. Nonlinear Dynamic Buckling of Asymmetrical Suspended Roofs under Step Loading. Computational Mechanics J. 21 (4–5), 389–397.

Milnor, J., 1985. On the concept of attractor. Comm. Math. Phys. 99, 177–195.

Moser, J., 1968. Lectures on Hamiltonian systems, Mem. Amer. Math. Soc. 81, American Mathematical Society, Providence.

Parker, T.S., Chua, L.O., 1987. Chaos: A Tutorial for Engineers. Proceedings of the IEEE 75 (8), 982–1007.

Ruelle, J., 1981. Small random perturbations of dynamical systems and the definition of attractors. Comm. Math. Phys. 82, 137–151.

Wiggins, S.T., 1980. Introduction to Applied Nonlinear Dynamical Systems and Chaos, Springer-Verlag, New York.